Brownian Diffusion of Hexagonal Boron Nitride Nanosheets and Graphene in Two Dimensions

Utana Umezaki,[1, ▽] Ashleigh D. Smith McWillams,[1, ▽] Zhao Tang,[2] Zhi Mei Sonia He,[1] Ivan R. Siqueira,[2] Stuart J. Corr,[3,4] Hijun Ryu,[1] Anatoly B. Kolomeisky,[1]* Matteo Pasquali,[1,2,5]* Angel A. Martí[1,4,5]*

[1] Department of Chemistry, Rice University, Houston, Texas 77005, United States
[2] Department of Chemical and Biomolecular Engineering, Rice University, Houston, Texas 77005, United States
[3] Department of Cardiovascular Surgery, Houston Methodist Hospital, Houston, Texas 77030, United States
[4] Department of Bioengineering, Rice University, Houston, Texas 77005, United States
[5] Department of Materials Science & Nanoengineering, Rice University, Houston, Texas 77005, United States
[▽] Co-first author
*Corresponding Author: tolya@rice.edu, mp@rice.edu, amarti@rice.edu

Abstract

Two-dimensional (2D) nanomaterials have numerous interesting chemical and physical properties that make them desirable building blocks for the manufacture of macroscopic materials. Liquid-phase processing is a common method for forming macroscopic materials from these building blocks, including wet-spinning and vacuum filtration. As such, assembling 2D nanomaterials into ordered functional materials requires understanding their solution dynamics. Yet, there are few experimental studies investigating the hydrodynamics of disk-like materials. Herein, we report that the lateral diffusion of hexagonal boron nitride nanosheets (h-BN and graphene) in aqueous solution. This was done by imaging fluorescent surfactant-tagged nanosheets and visualizing them using fluorescence microscopy. Spectroscopic studies were conducted to characterize the interactions between h-BN and the fluorescent surfactant and atomic force microscopy (AFM) to characterize the quality of the dispersion. The diffusion data under different gap sizes and viscosities displayed a good correlation with Kramers' theory. We propose that the yielded activation energies by Kramers' equation express the magnitude of the interaction between fluorescent surfactant tagged h-BN and glass because the energies remain constant with changing viscosity and decrease with increasing confinement size. The diffusion of graphene presented a similar trend with similar activation energy as the h-BN. This relationship

suggests that Kramers' theory can also be applied to simulate the diffusion of other two-dimensional nanomaterials.

Keywords Hexagonal boron nitride (h-BN) nanosheets, Graphene, Brownian motion, Translational diffusion, Fluorescence microscopy, Kramers' theory

Introduction

Two-dimensional (2D) nanomaterials, such as graphene,[1] hexagonal boron nitride (h-BN),[2] and transition metal dichalcogenides (TMDCs),[3] compose an important subgroup of nanomaterials with exciting and novel properties. Due to their valuable mechanical, thermal, and electronic properties, they have been proposed for a wide variety of applications, including energy storage, protective films, and electronics, among others.[4,5] Reaching these important applications relies heavily on our ability to use liquid-phase processing to manufacture highly ordered macroscopic materials from these nanosheet building blocks, given their properties depend on the alignment of nanosheets.[6–8] While there have been some studies on aligning 2D nanomaterials,[6–11] very little work has been done toward a fundamental understanding of the behavior of such systems in solution. Theoretical predictions have been proposed for disk-like particle diffusion through a bulk solution;[12,13] however, to the best of our knowledge, little experimental work has been done at the single sheet level,[14] with most work performed using bulk such as dynamic light scattering (DLS).[15–18] On the other hand, for rigid rods, experimental studies on model rods, such as actin filaments,[19] carbon nanotubes (CNTs),[20] germanium nanowires,[21] and boron nitride nanotubes (BNNTs),[22] were utilized to determine and confirm a model of Brownian rod-like particle diffusion through a confined solution. These results were utilized to accelerate the understanding of the behavior and diffusion of rod-like particles in biological systems and in the production of materials from rigid rod building blocks, such as CNTs.[23–28] In each of these systems, the rigid rod particles were studied on the single-molecule level to understand how changes in rod length impact diffusivity. Additionally, each system was studied under confinement, as a confinement model is more applicable to both biological systems[24] and materials processing.[29] To date, this level of understanding has not been accessed for disk-like materials.

Herein, we use h-BN as a model 2D nanomaterial for translational diffusion studies under confinement. h-BN is a structural allotrope of graphene, with alternating boron and nitrogen atoms

forming a honeycomb structure in two dimensions.[2] In addition to being lightweight and mechanically strong, similar to graphene, h-BN is also chemically inert, thermally stable, and electrically insulating.[2,30–32] In this study, we aim to gain insight into the unexplored hydrodynamics of h-BN with direct observation of its lateral diffusivity (x and y directions in Figure 1) in confined geometries. Since h-BN is transparent to visible light, we utilize a rhodamine-based surfactant and fluorescence microscopy, as previously reported for BNNTs,[22,33] to visualize each h-BN sheet. The z-direction of h-BN diffusion is confined between glass slides using silica microspheres to control the gap size. The isothermal translational diffusion coefficients of many h-BN sheets suggest that h-BN diffusion in two dimensions can be effectively described using Kramers' rate theory. Besides h-BN size variation experiments, diffusivities under different viscosities and confinement sizes follow the theory. Furthermore, we demonstrate that the diffusion behavior of graphene is similar to h-BN. We expect the results of this study will be applicable to understanding the behavior of a variety of 2D materials, advancing our understanding of their dynamics in solution and facilitating their processing into advanced macroscopic materials.

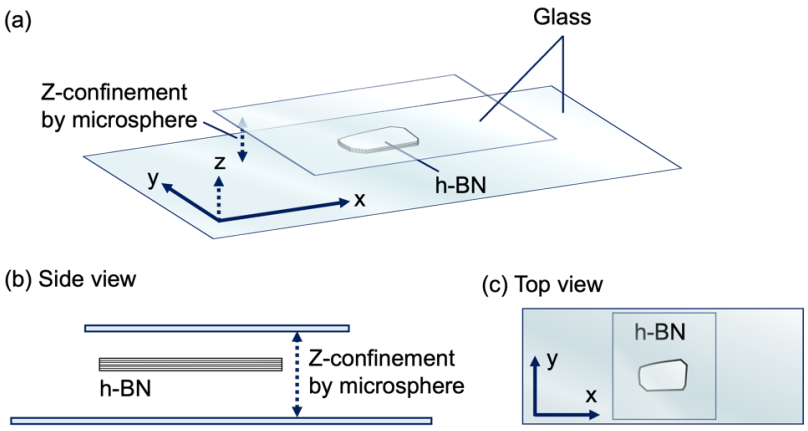

Figure 1. Schematic image of the pictorial h-BN imaging sample. To avoid complexity, we ignored the R12/CTAC solution and silica microspheres here and the h-BN sheet size has been enlarged (not to scale). (a) Overall system. (b) Side view of (a). (c) Top view of (a).

Results and Discussion

Interactions of R12 with h-BN

To study the interactions of R12 with h-BN, we employed UV-Vis spectroscopy as well as steady-state and time-resolved photoluminescence spectroscopy. The samples for these studies

were not centrifuged after sonication to have a reasonable concentration of h-BN facets interacting with R12. Additionally, dialysis with DI water was used to remove a great portion of free R12, leaving a sample enriched in R12 interacting with h-BN. Figure 2a and b show the absorbance and steady-state photoluminescence spectra of the dialyzed sample, respectively. Both spectra are consistent with those observed for R12 in the presence of BNNTs.[22] Figure 2c shows the fluorescence lifetime decay of the dialyzed sample. The decay traces of free R12 (no h-BN) yield a mono-exponential decay with a lifetime of 2076 ps. On the other hand, the decay traces of the dialyzed sample result in a tri-exponential decay with τ_1 = 209 ps (43.2 %), τ_2 = 871 ps (30.4 %), and τ_3 = 2076 ps (26.4 %). Obviously, the longest lifetime component arises with the free R12. We assume that the interaction between h-BN and R12 causes the two shorter lifetime components. Previous study with BNNTs reported only one additional lifetime component, τ = 240 ps.[22] It is expected that τ_1 and τ_2 represent two different binding environments of R12, consistent with R12 interacting with the hBN basal plane and interacting with the hBN edge and defect sites, respectively. Several studies about molecular edge termination of h-BN after the liquid exfoliation process suggest its boron terminal can be functionalized with hydroxyl groups.[34,35] Using the knowledge of the relative percentages of bound (73.6 %) and free R12 (26.4 %), we calculated an average quantum yield of R12 bound to h-BN (see supporting information for details). The calculated quantum yield of bound R12 to h-BN is 0.036, which is considerably smaller than the quantum yield of free R12 (0.26).[22] The change in quantum yield of R12 after binding suggests a close interaction between the rhodamine head and h-BN, resulting in the additional nonradiative decay of excited R12, likely due to pi stacking.

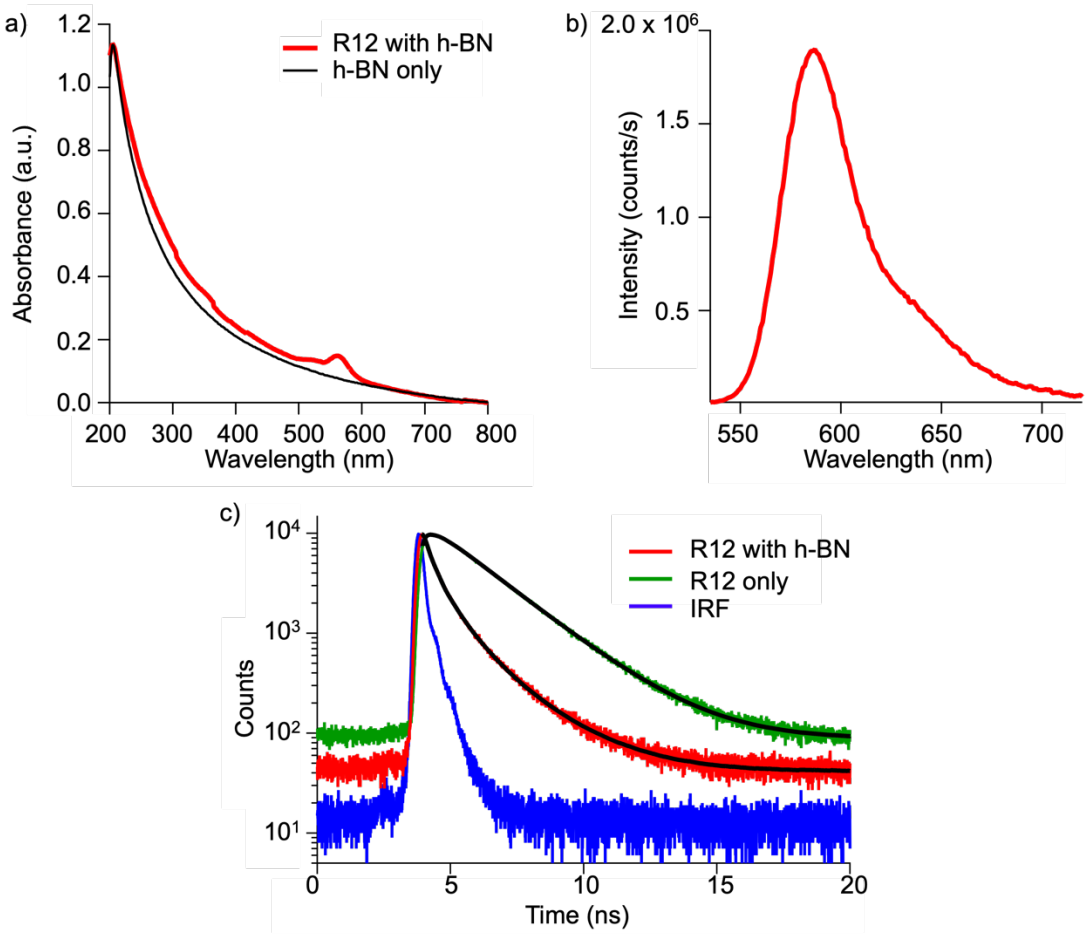

Figure 2. Various spectra of R12 in the presence of h-BN (a) Absorbance spectrum (black line is the scattering background of h-BN in CTAC). (b) Steady-state photoluminescence spectrum. (c) Photoluminescence lifetime decay of R12 with h-BN (red), R12 (green), and instrument response function (blue).

Characterization of exfoliated h-BN sheets

AFM imaging of the h-BN sheets was used to determine their thickness and assess the efficiency of the dispersion and exfoliation steps (Figure 3). Yellow particles in the AFM image are remained surfactants from the rinsing step at the sample preparation.[36] AFM height measurements of 99 randomly chosen h-BN sheets show an average sheet thickness of 5.5 ± 0.6 nm. Considering that the interlayer distance of h-BN is 0.33 nm,[37] the height indicates that approximately 17 layers of h-BN were produced by our exfoliation procedure. This AFM study demonstrates that h-BN sheets were well-dispersed and exfoliated uniformly by our sample preparation.

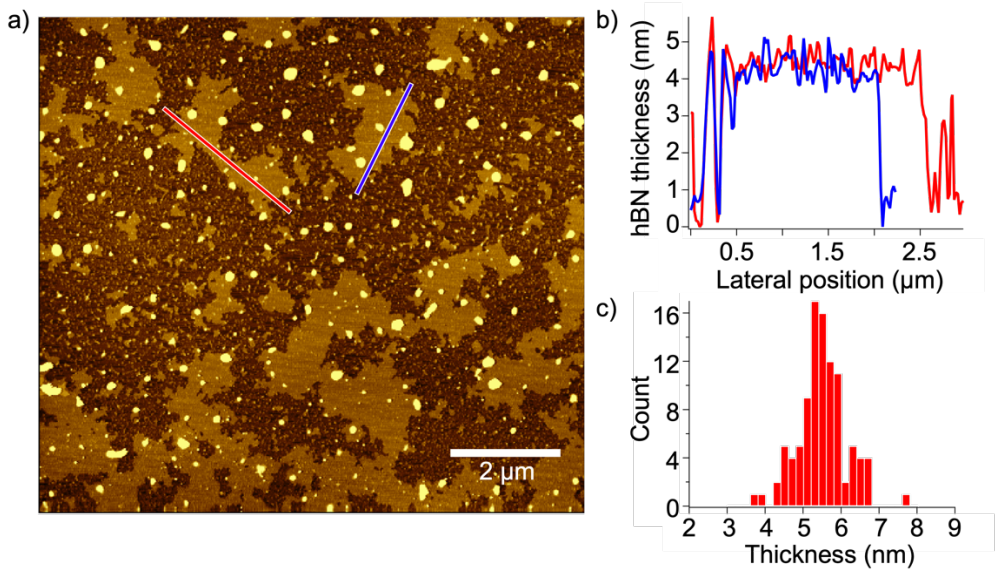

Figure 3. (a) Representative AFM image of dispersed h-BN sheets. (b) Height profiles from two sample h-BN sheets. (c) Histogram with 0.2 nm width bins showing the average thicknesses (5.5 ± 0.6 nm) of 99 randomly chosen h-BN sheets.

Area-dependent diffusion studies of h-BN

The exfoliated and fluorescently tagged h-BN sheets were mixed with 2 μm silica microspheres before being added to the microscope slide. These microspheres created a uniform, 2 μm confinement between the slide and coverslip. The coverslip was sealed with epoxy to prevent any convective flow of the h-BN sheets, ensuring only the observation of their Brownian motion. Figure 4 presents time-lapse images showing the diffusion of an 18.9 μm^2 h-BN sheet. The brightness contrast on the h-BN sheet might arise due to the chemical differences on the surface and edge/defects,[34,35] as inferred from the lifetime data, or by an uneven distribution of surfactant molecules on the surface of h-BN.

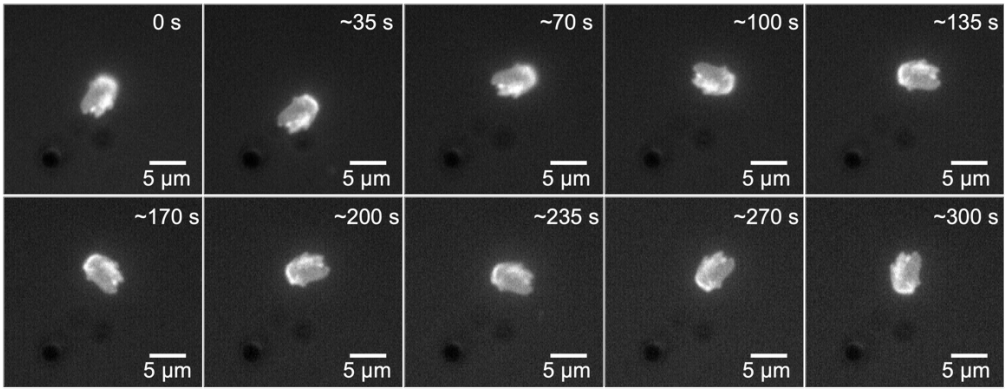

Figure 4. Time-lapse images of an 18.9 µm^2 h-BN sheet undergoing Brownian motion under the 2 µm confinement. The dark non-diffusing sphere on the bottom left corner is a 2 µm silica microsphere.

The position of the h-BN center of mass was measured for each frame and plotted as a function of time. Figure 5a shows representative trajectories obtained for the 18.9 µm^2 h-BN sheet. These trajectories were used to calculate the mean-squared displacement (MSD) of the h-BN sheet (Figure 5b). Displacements were obtained using internal averaging, so all position pairs within the same time interval were included for each point.[38] The MSD curve was used to calculate the translational diffusion coefficient (D_t). Movement in the z-direction was limited by only analyzing sheets with areas larger than the confinement gap size (2 µm), so the translational diffusion could be measured in two dimensions. In addition, the observed lateral translational motion could be assumed to be a mostly edge-on (parallel) rather than a face-on (perpendicular) orientation of the sheets. Therefore, the diffusion coefficients of h-BN were determined using a relationship between MSD in two dimensions and lag time, MSD = $4D_t\Delta t + C$, where the constant C comes from uncertainty in the measurements due to the microscope's resolution and exposure time. All measurements had an uncertainty of less than 0.1 µm^2, and the error of D_t was less than 1 %.

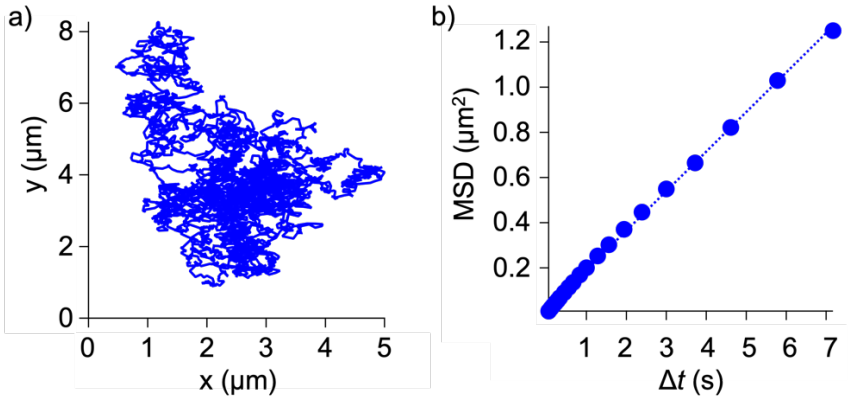

Figure 5. (a) Example analysis of an 18.9 μm^2 h-BN sheet shows the position of the center of mass. (b) The mean squared displacement over time. Only the linear portion of the MSD graph is shown. The slope of the MSD graph equals $4D_t$.

Translational diffusion coefficients were extracted from trajectories for h-BN sheets with areas ranging from ~ 2 to 20 μm^2. Figure 6 shows the translational diffusion coefficients under 2 μm confinement plotted as a function of h-BN sheet areas. Plotting these values in a linear-linear scale clearly shows that D_t decreases with increasing sheet area. It is paramount to note that in these experiments, the h-BN nanosheets were covered with cationic surfactants, including R12 and CTAC, which interact with the glass surface. Indeed, when we cleaned the slides and coverslips with Piranha solution, which added hydroxy groups to the glass, most of the h-BN sheets adhered to the glass surface. This observed interaction motivated us to utilize Kramers' approach to fit our data. Kramers' theory is one of the major approaches to describe a transition between two local energy minima, originally developed as a reaction rate theory.[41,42] This theory has been expanded to express protein folding dynamics,[43–45] the diffusion of particles between a dual optical trap,[46,47] and surface diffusion.[48,49] By following Kramers' theory, the diffusion coefficient is expected to follow an Arrhenius type equation:[49]

$$D_{\mathrm{t}} = D_0 \exp\left(-\frac{E_a}{k_B T}\right) = D_0 \exp\left(-\frac{aS}{k_B T}\right) \quad (1)$$

where D_{t} is the translational diffusion coefficient determined with MSD analysis, D_0 is the pre-exponential factor, E_a is the activation energy for a single h-BN sheet to dissociate before diffusion, a is activation energy per unit area of a single h-BN sheet, S is the area of the h-BN sheet, k_B is the Boltzmann constant, and T is temperature. The hypothesis is that for h-BN to move, the sheet (which is composed of the h-BN sheet and the cationic surfactants enveloping it) has to break interactions with the glass surface (partially desorbing) and diffuse until adsorbed again at a different location. This effectively corresponds to motion between two free-energy minima. This means that, for an h-BN particle to diffuse in this system, the cationic surfactant-coated h-BN has to overcome the energy barriers created by interactions of the h-BN/surfactants with the glass surface. The fitted line is shown as a dashed line resulting in values of D_0 = 0.35 μm^{2}s^{-1} and a = 4.7×10^{-22} Jμm^{-2} (Table 1(b)). The good agreement between the data and the curve obtained from

equation 1 suggests that Kramers' theory indeed can be used to accurately describe the diffusion of nanosheets in two dimensions.

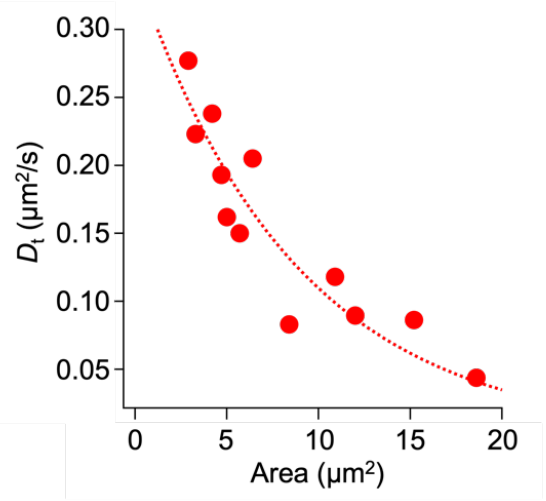

Figure 6. Plot of translational diffusion coefficients of h-BN sheets under 2 μm confinement plotted as a function of sheet area. The dashed line is a non-linear least square fit to equation 1.

Jańczuk *et al.* reported the free energy of adsorption of cetyltrimethylammonium bromide (CTAB) between a glass-solution interface as -31.51 kJmol^{-1} (5.232×10^{-20} J).[50] Compared to our yielded activation energy, the reported adsorption free energy was significantly larger. This can be explained by considering that the activation barrier for the movement of h-BN in our system is a hydrodynamic interaction due to the topology of the glass surface. We presume that the difference in the adsorption free energy is because our system is a transition between two states (where there is a hydrodynamic interaction between h-BN and the glass), while the reported value is the transition between free and adsorbed states. In our experiments, we often encounter h-BN sheets that do not move at all, and therefore are truly adsorbed to the glass. It is likely that given enough time, all h-BN sheets will get irreversibly adsorbed to the glass slides. Figure 7 is the proposed energy diagram of our system. The absolute value of activation energy depends on the area of the h-BN sheet, the total number of surfactant molecules on the h-BN sheet, and the number of hydroxyl groups on the glass surface.

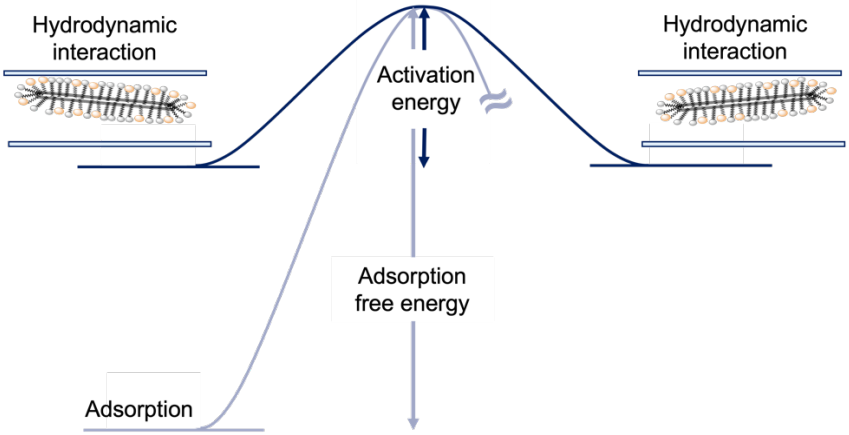

Figure 7. Schematic image of energy states and cross-section of our sample at each energy state. Gray spheres with 16 carbon alkyl chains represent CTAC, and orange spheres with 12 carbon alkyl chains represent R12. Solution and microspheres are ignored in this image. The dark blue line shows two local minima corresponding to the state where surfactants on the h-BN sheet interact with the glass coverslip at different locations. The activation energy calculated by Kramers' theory is depicted by the local maxima in the diagram. The light blue line shows an adsorption state, which is lower than our observed activation energy.

To further investigate the diffusion behavior of h-BN, a set of experiments were performed under a variety of conditions, including varying size confinement and viscosity. Figure 8(a) shows the diffusion coefficients of different size h-BN sheets under 1, 2, and 4.5 μm gaps, which were effectively fitted to equation 1. Figure 8(a) shows the diffusion coefficients of different size h-BN sheets under 1, 2, and 4.5 μm gaps, which were effectively fitted to equation 1. The D_0 and a values for the different gap sizes can be found in Table 1. While the D_0 value for the 1 μm gap looks larger than the larger gaps, the uncertainty is also large. Actually, all D_0 have overlapping error bars and can be considered as undistinguishable within error at this point. In terms of activation energies, it can be noticed that these decrease with increasing gap sizes, which suggests lesser interactions between h-BN and the glass surface when the distance between the glass slides is increased. The smaller the gap, the higher the probability that h-BN will diffuse close to the wall on either side. The effect of viscosity on the diffusion coefficients is shown in Figure 8(b). The viscosity of the solution without the sucrose/glucose mixture was 1.22×10^{-3} Pa·s. In contrast, the solution's viscosity with the 40 wt% sucrose/glucose mixture was 5.13×10^{-3} Pa·s, a *ca.* 4-fold increase. The D_0 value decreased by a factor of *ca.* 6, approximately proportional to the increasing viscosity, while the a value remained unchanged between different viscosity samples (Table 1(b) and (d)). The activation energy should not change with viscosity change. According to Kramers' argument, the viscosity should only affect the pre-exponential factor.[41] The similar activation

energies suggest the interaction between h-BN/surfactants and glass does not change significantly with changing viscosity, further validating the use of Kramers' theory to describe the diffusion of h-BN under confinement.

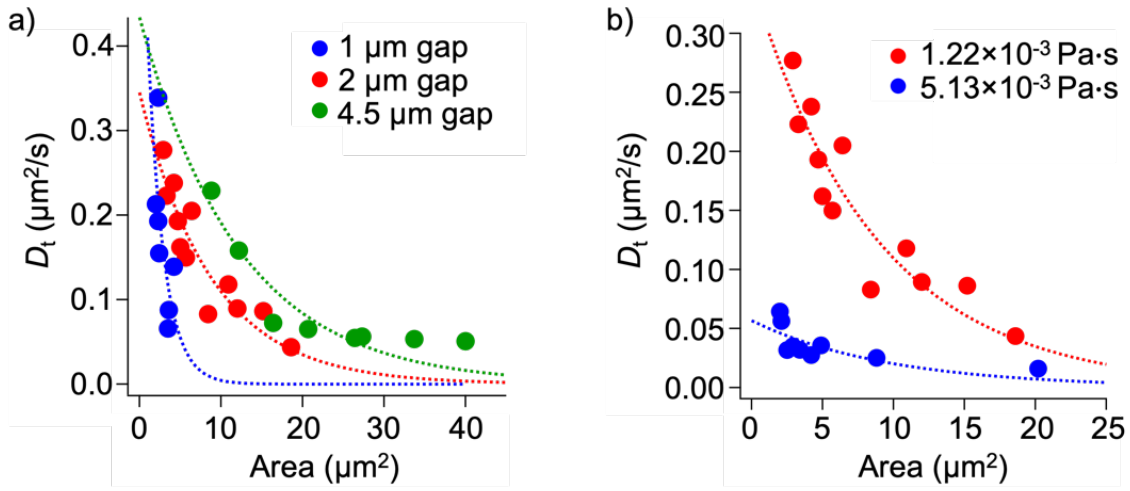

Figure 8. Linear-linear plots of translational diffusion coefficients of various sizes of h-BN sheet under different conditions. (a) Translational diffusion coefficients of h-BN sheets under 1 μm confinement (blue), 2 μm confinement (red), and 4.5 μm confinement (green) plotted as a function of sheet area. (b) Translational diffusion coefficients of h-BN sheets under 2 μm confinement in a high viscosity solution (blue) plotted as a function of sheet area.

Table 1. D_0 and a values determined from various areas of h-BN diffusion under 4 different conditions: (a) 1 μm gap, (b) 2 μm gap, (c) 4.5 μm gap, (d) 2 μm gap with high viscosity. All experiments were performed at room temperature.

	Gap size	Viscosity (Pa·s)	D_0 (μm^{2}s^{-1})	a (Jμm^{-2})*
a)	1 μm	1.22×10^{-3}	0.7 ± 0.47	2×10^{-21}
b)	2 μm	1.22×10^{-3}	0.35 ± 0.039	4.7×10^{-22}
c)	4.5 μm	1.22×10^{-3}	0.43 ± 0.096	3.5×10^{-22}
d)	2 μm	5.13×10^{-3}	0.06 ± 0.012	4.4×10^{-22}

*The temperature used to calculate the activation energies per area was assumed to be 22 °C

Area-dependent diffusion study of graphene

In addition to h-BN, we tracked graphene nanosheets to investigate whether Kramers' theory could be generalized for other 2D nanomaterials. AFM studies indicate that our dispersion and exfoliation procedure using CTAC and R12 surfactants in solution is effective for graphite (Figure 9). AFM height measurements of 85 randomly chosen graphene sheets show an average

sheet thickness of 1.5 ± 0.3 nm. The thickness of a single layer of graphene is 0.335 nm;[31] the height indicates approximately four layers of graphene on average per diffusing nanosheet.

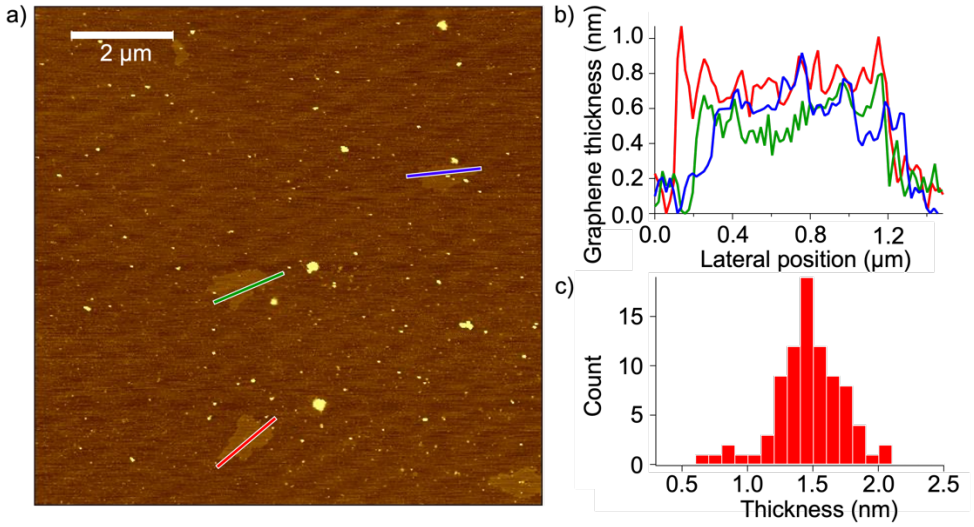

Figure 9. (a) Representative AFM image of dispersed graphene sheets. (b) Height profiles of three sample graphene sheets. (c) Histogram with 0.1 nm width bins showing the average thicknesses of 85 randomly chosen graphene sheets.

Figure 10(a) is a time-lapse image of the diffusion of a 7.4 μm^2 graphene sheet under a 2 μm confinement, and Figure 10(b) shows the MSD of the sheet over lag time. We observed ~2.5-15 μm^2 graphene sheets under 2 μm confinement and plotted the diffusion coefficients as a function of sheet areas in Figure 11. Interestingly, the a value of graphene was approximately the same as that calculated for h-BN, as shown in Table 2. The similar values suggest that interactions with the glass surface occur in both h-BN and graphene and are non-specific to the chemical nature of the diffusing particle. This observation is likely dominated by the presence of a similar surfactant shell in both nanomaterials. The consistency between two different 2D nanomaterials supports that these results would be applicable to other nanosheet species, even we expect limitations using this Kramers' equation, including the case of anomalous diffusions, different surface structure of the 2D nanomaterials, and symmetry of the 2D nanomaterials' shapes. The slight difference in diffusion coefficients might arise from the discrepancy in flexibility due to sheet thickness between the h-BN and graphene sheets. It is known that h-BN nanosheets are stiffer than graphene,[51] and actually, in the video (SV1), the graphene sheet seems to be wrinkling while diffusing. In the case of rodlike nanostructures, studies indicate that

flexible nanorods show slower diffusivity when compared to rigid ones.[52] We suggest that smaller D_0 of thinner graphene arises from the additional degrees of freedom due to the flexibility of the sheetlike nanostructures, making the diffusion slower as observed for rodlike particles. We hypothesize that graphene flexibility allows for the nanosheet to redistribute energy from solvent collisions locally without changing the center of mass (*i.e.*, wrinkling). Furthermore, the slower diffusivity of graphene suggests the thickness of 2D nanomaterials plays a relatively smaller role in our system. Notably, the diffusion coefficients of both h-BN and graphene are comparable with the previously reported DLS measurement of translational diffusion coefficients of similar 2D nanomaterial, graphene oxide,[17] although slightly lower. Bulk measurements such as DLS give averaged properties and hence are not expected to match exactly with single-molecule experiments. We note that the slight differences in diffusion coefficient may be due to wall-induced drag originating from the proximity of the glass slide and coverslip, as narrow gaps are known to increase the effect of hydrodynamic drag in particle diffusion.[20]

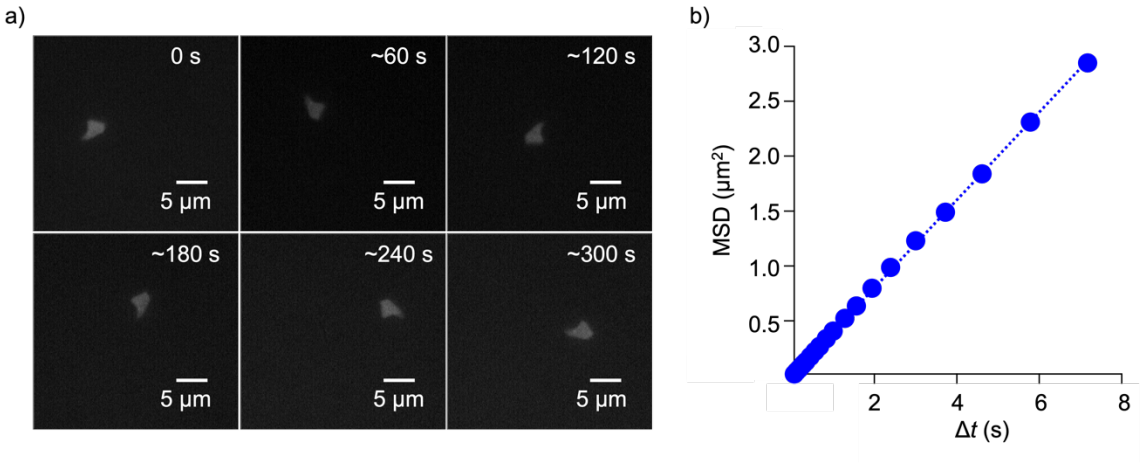

Figure 10. (a) Time-lapse images of a 7.4 μm^2 graphene sheet undergoing Brownian motion under a 2 μm confinement. (b) The mean squared displacement over time.

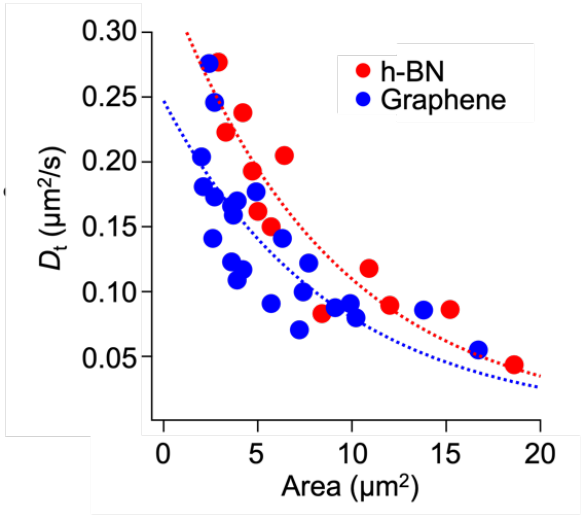

Figure 11. Linear-linear plots of translational diffusion coefficients of h-BN sheets (blue circles) and graphene sheets (red circles) under 2 μm confinement are plotted as a function of sheet area.

Table 2. Comparison of D_0 and a values of h-BN and graphene.

	Material	D_0 ($\mu m^2 s^{-1}$)	a ($J\mu m^{-2}$)*
a)	h-BN	0.35 ± 0.039	4.7×10^{-22}
b)	Graphene	0.25 ± 0.026	4.7×10^{-22}

*The temperature used to calculate the activation energies per area was assumed to be 22 °C

Conclusions

In summary, diffusion of a model sheet, h-BN, under z-axis confinement has been directly observed and investigated. The interaction between R12 and h-BN was confirmed with spectroscopic studies. Photoluminescence lifetime experiments indicate two different binding environments of R12 on h-BN. AFM studies provide evidence that the h-BN samples were sufficiently dispersed and exfoliated to perform imaging experiments. Diffusion studies of h-BN sheets with different surface areas can be described by Kramers' theory. A Kramers' theory-based analysis of h-BN diffusion yields ideal diffusion coefficients and activation energy per area of a single sheet. We presume the activation energy is related to the amount of energy needed for moving the h-BN sheet between different locations in the system that exhibit similar interactions. This is due to the constant activation energy regardless of viscosity, while activation energy

decreases with increasing gap size. Furthermore, the obtained activation energy for graphene is similar to that of h-BN, which supports our expectation that these results will be applicable to other nanosheet species, including the diffusion of TMDCs. Future work will be necessary to determine an exact mathematical model for the translational diffusion of confined nanosheets due to the limitations of using simple Kramers' equation. Still, we believe all insights in this report provide a significant step toward understanding the hydrodynamics of 2D nanomaterials. As was realized with rigid rods,[23–28] this knowledge could be central for manipulating liquid-phase processing techniques to produce macroscopic materials. Additionally, this would be important in understanding the dynamics of 2D nanomaterials after introduction into biological systems, such as in drug nanocarriers.[53]

Methods

Materials. h-BN was obtained from US Nano and used as received. Cetyltrimethylammonium chloride (CTAC) was purchased from BTC. Rhodamine surfactant with 12 alkyl chains (R12) was synthesized by a previously reported method.[22,33] Glass slides and coverslips were purchased from Thermo Scientific, washed with isopropanol, and air-dried before use.

Preparation of R12-tagged h-BN samples. A *ca.* 2 mM solution of the rhodamine surfactant in methanol was prepared. This was diluted 35 times with a 1 wt. % CTAC solution for a final rhodamine surfactant concentration of *ca.* 5.7 μM. 0.5 mg of h-BN and 7 mL of the surfactant mixture were added to a 20 mL glass vial containing a stir bar. The solution was stirred overnight and bath ultrasonicated (Cole-Parmer 8891, 42 kHz) for 20 minutes to disperse and exfoliate the h-BN sheets from the stacked material. The resulting suspension was centrifuged at 2,500 *g* for 30 minutes to remove large aggregates, and the supernatant was collected for atomic force microscopy (AFM) and fluorescence microscopy studies.

Spectroscopic studies of R12-tagged h-BN. Spectroscopic study samples were prepared from R12-tagged h-BN without centrifuging. The dispersed and exfoliated sample was dialyzed against deionized (DI) water for 15 hours with a dialysis cassette (MWCO 10,000) to remove excess rhodamine surfactant not attached to h-BN. Absorbance and scattering measurements were performed using a Shimadzu 2450 UV-visible spectrophotometer. The steady-state fluorescence intensity of the sample was measured with a Horiba Nanolog Spectrophotometer. The sample was

excited at 514 nm, and its emission was recorded from 535 to 720 nm. Time-resolved decays were recorded using an Edinburgh Instruments OD470 single photon counting spectrometer with a 374 nm picosecond pulse diode laser with a high-speed red detector. The sample was excited at 375 nm and recorded at 610 nm. The standard used for calculating quantum yield was Ar purged $[Ru(bpy)_3]Cl_2$ in water, which has a known absorbance and integrated photoluminescence (λ_{ex} = 514 nm, λ_{em} = 535 – 800 nm). The quantum yield of the Ar purged $[Ru(bpy)_3]Cl_2$ under these conditions was considered as 0.063.[54]

AFM height studies of h-BN. AFM samples were prepared by depositing samples on a freshly cleaved mica surface primed with 20 mM $MgCl_2$. The mica surface was heated to ~120˚C using a hot plate, and the dispersion was applied through a spray bottle in order to deposit a fine mist that could quickly dry. Excess surfactant was removed by rinsing in water without agitation. The same depositing process was repeated, followed by rinsing the sample in water and isopropanol before leaving the samples to dry in an oven at 110˚C for 1 hour. AFM measurements were performed with a Digital Instruments Nanoscope IIIa scanning probe microscope controller in tapping mode. AFM images were processed in Gwyddion, and the height profiles of 99 randomly selected h-BN sheets were collected.

Preparation of h-BN microscope samples. 0.5-1.5 μL of silica microspheres suspension (1, 2, or 4.5 μm, Bangs Laboratories) were added to 100 μL of the R12 tagged h-BN solution. For imaging, 0.6 μL of the h-BN and microspheres mixture were placed between a microscope slide and a coverslip, both of which were pre-cleaned with isopropanol. The sample was then sealed with epoxy to prevent convective flow due to solvent evaporation. High viscosity samples were prepared by adding a 60:40 sucrose/glucose mixture, for a final concentration of 40 wt%, with the R12 tagged h-BN sample following a procedure reported previously.[55]

Imaging h-BN. The tagged h-BN sheets were imaged on a Zeiss Axiovert 200M epi-fluorescence microscope with a TRITC (Rhodamine B) filter cube (Chroma; λ_{ex} 527-552/ 565 dichroic/ λ_{em} 577-632 nm), a 100x oil immersion objective (N.A.=1.3; diffraction limit (d) ≈ 200 nm), and a Toupcam industrial digital camera with a 1.4MP Sony CCD sensor (~18 frames per second), controlled by ToupView software. Videos were collected for approximately ~5 minutes (~5,400 frames). The position of the h-BN center of mass was determined by averaging the x and y pixel information of h-BN.

Imaging graphene. R12-tagged graphene was prepared using the same procedure utilized for h-BN, except using graphite instead of h-BN. Graphite powder was obtained from Sigma-Aldrich and used as received. The R12-tagged graphene was prepared following the same procedure and using the same equipment as for the h-BN samples. Briefly, a *ca*. 2 mM of R12 in methanol was diluted 35 times to make the final concentration of R12 as *ca*. 5.7 μM using a 1 wt. % CTAC solution. 0.5 mg of graphite was added to the 7 mL of surfactant mixture. The graphite and surfactant mixture was stirred overnight and bath ultrasonicated for 20 min to disperse and exfoliate the graphene from the graphite. The sonicated sample was centrifuged at 2,500 g for 30 min and the supernatant was used for the AFM height study and the fluorescence microscope study. The graphene sample for AFM measurement was prepared using similar procedures to the h-BN samples. A freshly cleaved mica surface primed with 20 mM $MgCl_2$ was heated to ~120˚C using a hot plate, and the R12-tagged graphene sample was sprayed on the mica. Excess surfactant was washed away by rinsing in water and drying with air. The sample depositing process was repeated. Subsequently, the sample was rinsed in methanol before drying the sample in the oven at 100˚C for 1 hour. The AFM measurements and data processing were conducted using the same equipment and software as the h-BN height study. The height profiles of 85 randomly selected graphene were obtained. The graphene samples for diffusion study were prepared using the same process as the h-BN samples. In short, a mixture of 0.5 μL of 2 μm silica microspheres and 100 μL of R12-tagged graphene was prepared. 0.6 μL of the graphene and microspheres was placed between a microscope slide and a coverslip, both of which were pre-cleaned with isopropanol. The sample was sealed with epoxy. The sample was observed by the same instrumental setting up with the h-BN diffusion studies. The video was captured for approximately 5 minutes.

Acknowledgments

We acknowledge the financial support from the National Science Foundation (CHE-1807737 and CHE-2108838) and AFOSR (FA9550-19-1-7045). M.P. and A.B.K. also acknowledge the support from the Welch Foundation (C-1668 and C-1559).

Supporting Information Available:

An averaged quantum yield calculation of R12 bound to h-BN (PDF)

Video of a 7.4 μm^2 graphene diffusion (AVI)

References

(1) Mohan, V. B.; Lau, K.; Hui, D.; Bhattacharyya, D. Graphene-Based Materials and Their Composites: A Review on Production, Applications and Product Limitations. *Compos. Part B Eng.* **2018**, *142*, 200–220.

(2) Golberg, D.; Bando, Y.; Huang, Y.; Terao, T.; Mitome, M.; Tang, C.; Zhi, C. Boron Nitride Nanotubes and Nanosheets. *ACS Nano* **2010**, *4*, 2979–2993.

(3) Coleman, J. N.; Lotya, M.; O'Neill, A.; Bergin, S. D.; King, P. J.; Khan, U.; Young, K.; Gaucher, A.; De, S.; Smith, R. J.; Shvets, I. V.; Arora, S. K.; Stanton, G.; Kim, H.-Y.; Lee, K.; Kim, G. T.; Duesberg, G. S.; Hallam, T.; Boland, J. J.; Wang, J. J.; et al. Two-Dimensional Nanosheets Produced by Liquid Exfoliation of Layered Materials. *Science* **2011**, *331*, 568–571.

(4) Tan, C.; Cao, X.; Wu, X.-J.; He, Q.; Yang, J.; Zhang, X.; Chen, J.; Zhao, W.; Han, S.; Nam, G.-H.; Sindoro, M.; Zhang, H. Recent Advances in Ultrathin Two-Dimensional Nanomaterials. *Chem. Rev.* **2017**, *117*, 6225–6331.

(5) Huang, H.; Sheng, X.; Tian, Y.; Zhang, L.; Chen, Y.; Zhang, X. Two-Dimensional Nanomaterials for Anticorrosive Polymeric Coatings: A Review. *Ind. Eng. Chem. Res.* **2020**, *59*, 15424–15446.

(6) Zhong, J.; Sun, W.; Wei, Q.; Qian, X.; Cheng, H.-M.; Ren, W. Efficient and Scalable Synthesis of Highly Aligned and Compact Two-Dimensional Nanosheet Films with Record Performances. *Nat. Commun.* **2018**, *9*, 3484.

(7) Wu, S.; Peng, S.; Wang, C. Multifunctional Polymer Nanocomposites Reinforced by Aligned Carbon Nanomaterials. *Polymers* **2018**, *10*, 542.

(8) Xin, G.; Zhu, W.; Deng, Y.; Cheng, J.; Zhang, L. T.; Chung, A. J.; De, S.; Lian, J. Microfluidics-Enabled Orientation and Microstructure Control of Macroscopic Graphene Fibres. *Nat. Nanotechnol.* **2019**, *14*, 168–175.

(9) Lin, Z.; Liu, Y.; Raghavan, S.; Moon, K.; Sitaraman, S. K.; Wong, C. Magnetic Alignment of Hexagonal Boron Nitride Platelets in Polymer Matrix: Toward High Performance Anisotropic Polymer Composites for Electronic Encapsulation. *ACS Appl. Mater. Interfaces* **2013**, *5*, 7633–7640.

(10) Lian, G.; Tuan, C.-C.; Li, L.; Jiao, S.; Wang, Q.; Moon, K.-S.; Cui, D.; Wong, C.-P. Vertically Aligned and Interconnected Graphene Networks for High Thermal Conductivity of Epoxy Composites with Ultralow Loading. *Chem. Mater.* **2016**, *28*, 6096–6104.

(11) Yu, C.; Gong, W.; Zhang, J.; Lv, W.; Tian, W.; Fan, X.; Yao, Y. Hot Pressing-Induced Alignment of Hexagonal Boron Nitride in SEBS Elastomer for Superior Thermally Conductive Composites. *RSC Adv.* **2018**, *8*, 25835–25845.

(12) Brenner, H. Rheology of a Dilute Suspension of Axisymmetric Brownian Particles. *Int. J. Multiph. Flow* **1974**, *1*, 195–341.

(13) Ortega, A.; García de la Torre, J. Hydrodynamic Properties of Rodlike and Disklike Particles in Dilute Solution. *J. Chem. Phys.* **2003**, *119*, 9914–9919.

(14) Maragó, O. M.; Bonaccorso, F.; Saija, R.; Privitera, G.; Gucciardi, P. G.; Iatì, M. A.; Calogero, G.; Jones, P. H.; Borghese, F.; Denti, P.; Nicolosi, V.; Ferrari, A. C. Brownian Motion of Graphene. *ACS Nano* **2010**, *4*, 7515–7523.

(15) Tawari, S. L.; Koch, D. L.; Cohen, C. Electrical Double-Layer Effects on the Brownian Diffusivity and Aggregation Rate of Laponite Clay Particles. *J. Colloid Interface Sci.* **2001**, *240*, 54–66.
(16) Kleshchanok, D.; Heinen, M.; Nägele, G.; Holmqvist, P. Dynamics of Charged Gibbsite Platelets in the Isotropic Phase. *Soft Matter* **2012**, *8*, 1584–1592.
(17) Kim, S. G.; Wang, S. H.; Ok, C. M.; Jeong, S. Y.; Lee, H. S. Lateral Diffusion of Graphene Oxides in Water and the Size Effect on the Orientation of Dispersions and Electrical Conductivity. *Carbon* **2017**, *125*, 280–288.
(18) Abele, C. D.; Giesselmann, F. Dynamic Light Scattering Analysis of Size-Selected Graphene Oxide 2D Colloids Fractioned *via* Liquid Crystal Phase Separation. *Soft Matter* **2022**, *18*, 6607–6617.
(19) Li, G.; Tang, J. X. Diffusion of Actin Filaments within a Thin Layer between Two Walls. *Phys. Rev. E* **2004**, *69*, 061921.
(20) Duggal, R.; Pasquali, M. Dynamics of Individual Single-Walled Carbon Nanotubes in Water by Real-Time Visualization. *Phys. Rev. Lett.* **2006**, *96*, 246104.
(21) Marshall, B. D.; Davis, V. A.; Lee, D. C.; Korgel, B. A. Rotational and Translational Diffusivities of Germanium Nanowires. *Rheol. Acta* **2009**, *48*, 589–596.
(22) Smith McWilliams, A. D.; Tang, Z.; Ergülen, S.; de los Reyes, C. A.; Martí, A. A.; Pasquali, M. Real-Time Visualization and Dynamics of Boron Nitride Nanotubes Undergoing Brownian Motion. *J. Phys. Chem. B* **2020**, *124*, 4185–4192.
(23) Reuel, N. F.; Dupont, A.; Thouvenin, O.; Lamb, D. C.; Strano, M. S. Three-Dimensional Tracking of Carbon Nanotubes within Living Cells. *ACS Nano* **2012**, *6*, 5420–5428.
(24) Fakhri, N.; MacKintosh, F. C.; Lounis, B.; Cognet, L.; Pasquali, M. Brownian Motion of Stiff Filaments in a Crowded Environment. *Science* **2010**, *330*, 1804–1807.
(25) Dan, B.; Ma, A. W. K.; Hároz, E. H.; Kono, J.; Pasquali, M. Nematic-Like Alignment in SWNT Thin Films from Aqueous Colloidal Suspensions. *Ind. Eng. Chem. Res.* **2012**, *51*, 10232–10237.
(26) Hussein, Z.; Rawson, F. J.; Oppenheimer, P. G.; Acton, A.; Mendes, P. M. Length-Selective Chemical Assembly of Vertically Aligned Carbon Nanotubes. *Adv. Mater. Interfaces* **2016**, *3*, 1500860.
(27) Mechrez, G.; Suckeveriene, R. Y.; Zelikman, E.; Rosen, J.; Ariel-Sternberg, N.; Cohen, R.; Narkis, M.; Segal, E. Highly-Tunable Polymer/Carbon Nanotubes Systems: Preserving Dispersion Architecture in Solid Composites via Rapid Microfiltration. *ACS Macro Lett.* **2012**, *1*, 848–852.
(28) Tang, Z.; Eichmann, S. L.; Lounis, B.; Cognet, L.; MacKintosh, F. C.; Pasquali, M. Single-Walled Carbon Nanotube Reptation Dynamics in Submicron Sized Pores from Randomly Packed Mono-Sized Colloids. *Soft Matter* **2022**, *18*, 5509–5517.
(29) Behabtu, N.; Young, C. C.; Tsentalovich, D. E.; Kleinerman, O.; Wang, X.; Ma, A. W. K.; Bengio, E. A.; ter Waarbeek, R. F.; de Jong, J. J.; Hoogerwerf, R. E.; Fairchild, S. B.; Ferguson, J. B.; Maruyama, B.; Kono, J.; Talmon, Y.; Cohen, Y.; Otto, M. J.; Pasquali, M. Strong, Light, Multifunctional Fibers of Carbon Nanotubes with Ultrahigh Conductivity. *Science* **2013**, *339*, 182–186.
(30) Li, L. H.; Chen, Y. Atomically Thin Boron Nitride: Unique Properties and Applications. *Adv. Funct. Mater.* **2016**, *26*, 2594–2608.

(31) Falin, A.; Cai, Q.; Santos, E. J. G.; Scullion, D.; Qian, D.; Zhang, R.; Yang, Z.; Huang, S.; Watanabe, K.; Taniguchi, T.; Barnett, M. R.; Chen, Y.; Ruoff, R. S.; Li, L. H. Mechanical Properties of Atomically Thin Boron Nitride and the Role of Interlayer Interactions. *Nat. Commun.* **2017**, *8*, 15815.
(32) Wang, J.; Ma, F.; Sun, M. Graphene, Hexagonal Boron Nitride, and Their Heterostructures: Properties and Applications. *RSC Adv.* **2017**, *7*, 16801–16822.
(33) Smith McWilliams, A. D.; Ergülen, S.; Ogle, M. M.; de los Reyes, C. A.; Pasquali, M.; Martí, A. A. Fluorescent Surfactants from Common Dyes – Rhodamine B and Eosin Y. *Pure Appl. Chem.* **2020**, *92*, 265–274.
(34) Lin, Y.; Williams, T. V.; Xu, T.-B.; Cao, W.; Elsayed-Ali, H. E.; Connell, J. W. Aqueous Dispersions of Few-Layered and Monolayered Hexagonal Boron Nitride Nanosheets from Sonication-Assisted Hydrolysis: Critical Role of Water. *J. Phys. Chem. C* **2011**, *115*, 2679–2685.
(35) Dorn, R. W.; Ryan, M. J.; Kim, T.-H.; Goh, T. W.; Venkatesh, A.; Heintz, P. M.; Zhou, L.; Huang, W.; Rossini, A. J. Identifying the Molecular Edge Termination of Exfoliated Hexagonal Boron Nitride Nanosheets with Solid-State NMR Spectroscopy and Plane-Wave DFT Calculations. *Chem. Mater.* **2020**, *32*, 3109–3121.
(36) Smith McWilliams, A. D.; Martínez-Jiménez, C.; Matatyaho Ya'akobi, A.; Ginestra, C. J.; Talmon, Y.; Pasquali, M.; Martí, A. A. Understanding the Exfoliation and Dispersion of Hexagonal Boron Nitride Nanosheets by Surfactants: Implications for Antibacterial and Thermally Resistant Coatings. *ACS Appl. Nano Mater.* **2021**, *4*, 142–151.
(37) Hod, O. Graphite and Hexagonal Boron-Nitride Have the Same Interlayer Distance. Why? *J. Chem. Theory Comput.* **2012**, *8*, 1360–1369.
(38) Saxton, M. J. Single-Particle Tracking: The Distribution of Diffusion Coefficients. *Biophys. J.* **1997**, *72*, 1744–1753.
(39) Streit, J. K.; Bachilo, S. M.; Naumov, A. V.; Khripin, C.; Zheng, M.; Weisman, R. B. Measuring Single-Walled Carbon Nanotube Length Distributions from Diffusional Trajectories. *ACS Nano* **2012**, *6*, 8424–8431.
(40) Michalet, X. Mean Square Displacement Analysis of Single-Particle Trajectories with Localization Error: Brownian Motion in an Isotropic Medium. *Phys. Rev. E* **2010**, *82*, 041914.
(41) Kramers, H. A. Brownian Motion in a Field of Force and the Diffusion Model of Chemical Reactions. *Physica* **1940**, *7*, 284–304.
(42) Hänggi, P.; Talkner, P.; Borkovec, M. Reaction-Rate Theory: Fifty Years after Kramers. *Rev. Mod. Phys.* **1990**, *62*, 251–341.
(43) Oliveberg, M.; Wolynes, P. G. The Experimental Survey of Protein-Folding Energy Landscapes. *Q. Rev. Biophys.* **2005**, *38*, 245–288.
(44) Kubelka, J.; Henry, E. R.; Cellmer, T.; Hofrichter, J.; Eaton, W. A. Chemical, Physical, and Theoretical Kinetics of an Ultrafast Folding Protein. *Proc. Natl. Acad. Sci.* **2008**, *105*, 18655–18662.
(45) Chung, H. S.; Eaton, W. A. Single-Molecule Fluorescence Probes Dynamics of Barrier Crossing. *Nature* **2013**, *502*, 685–688.
(46) McCann, L. I.; Dykman, M.; Golding, B. Thermally Activated Transitions in a Bistable Three-Dimensional Optical Trap. *Nature* **1999**, *402*, 785–787.

(47) Curran, A.; Lee, M. P.; Di Leonardo, R.; Padgett, M. J. Hydrodynamic Assisted Barrier Escape. In *Optical Trapping and Optical Micromanipulation VIII*, *Proceedings of SPIE*, San Diego, California, USA, August 21-25, 2011; Dholakia, K., Spalding, G. C., Eds.; SPIE: Bellingham, Washington, USA, 2011; Vol. 8097, p 80970Q.
(48) Guantes, R.; Vega, J. L.; Miret-Artés, S.; Pollak, E. Kramers' Turnover Theory for Diffusion of Na Atoms on a Cu(001) Surface Measured by He Scattering. *J. Chem. Phys.* **2003**, *119*, 2780–2791.
(49) Fusco, C.; Fasolino, A. Nonlinear Dynamics and Surface Diffusion of Diatomic Molecules. *ChemPhysChem* **2005**, *6*, 1749–1752.
(50) Szymczyk, K.; Zdziennicka, A.; Jańczuk, B. Adsorption and Wetting Properties of Cationic, Anionic and Nonionic Surfactants in the Glass-Aqueous Solution of Surfactant-Air System. *Mater. Chem. Phys.* **2015**, *162*, 166–176.
(51) Qu, W.; Bagchi, S.; Chen, X.; Chew, H. B.; Ke, C. Bending and Interlayer Shear Moduli of Ultrathin Boron Nitride Nanosheet. *J. Phys. Appl. Phys.* **2019**, *52*, 465301.
(52) Doi, M. Effect of Chain Flexibility on the Dynamics of Rodlikk Polymers in the Entangled State. *J. Polym. Sci. Polym. Symp.* **1985**, *73*, 93–103.
(53) Zhang, H.; Fan, T.; Chen, W.; Li, Y.; Wang, B. Recent Advances of Two-Dimensional Materials in Smart Drug Delivery Nano-Systems. *Bioact. Mater.* **2020**, *5*, 1071–1086.
(54) Suzuki, K.; Kobayashi, A.; Kaneko, S.; Takehira, K.; Yoshihara, T.; Ishida, H.; Shiina, Y.; Oishi, S.; Tobita, S. Reevaluation of Absolute Luminescence Quantum Yields of Standard Solutions Using a Spectrometer with an Integrating Sphere and a Back-Thinned CCD Detector. *Phys. Chem. Chem. Phys.* **2009**, *11*, 9850–9860.
(55) Fakhri, N.; Tsyboulski, D. A.; Cognet, L.; Weisman, R. B.; Pasquali, M. Diameter-Dependent Bending Dynamics of Single-Walled Carbon Nanotubes in Liquids. *Proc. Natl. Acad. Sci.* **2009**, *106*, 14219–14223.